

## Heat and mass transfer simulation and experimental evaluation of solar powered vacuum membrane distillation system

Mohammad Ramezaniapour<sup>a</sup>, Muttucumaru Sivakumar<sup>b,\*</sup>

<sup>a</sup>Department of Engineering and Architectural Studies, Ara Institute of Technology, Christchurch, New Zealand

<sup>b</sup>GeoQuest Research Centre, School of Civil, Mining and Environmental Engineering, Faculty of Engineering and Information Sciences, University of Wollongong, Wollongong, NSW 2522, Australia, Tel. +(61) 2 4221 3055; email: siva@uow.edu.au

Received 10 December 2014; Accepted 19 June 2016

### ABSTRACT

Water and energy scarcity in dry and remote areas is a well understood issue and becoming even more pronounced in the future due to the impact of climate change. Research on solar powered desalination techniques in these places is growing worldwide to produce fresh water using renewable sources of energy. Membrane distillation processes are technically simple and capable of producing high-quality potable water over a long period with minimal maintenance. With regard to the attractive advantages of the vacuum membrane distillation (VMD) process, it is a promising technology that can be implemented by the use of solar energy. The aim of this paper is not only to develop a mathematical model describing heat and mass transfer processes across a VMD process using thermal renewable energy, but also to implement innovative design to improve the overall performance of a solar powered vacuum membrane distillation (SVMD) system. In the present work, a small pilot-scale SVMD unit was designed, assembled and tested. The dependency of the predictive model to natural climatic conditions is assessed and validated against experimental data. Theoretical flux data of the proposed SVMD pilot plant is then graphed via a numerical solution in order to compare with experimental results. The influence of salinity concentration on the permeate flux is explained. Finally, sensitivity analysis of the simulated model showed that the permeate flux is highly sensitive to pressure, solar irradiance and flow rate values.

*Keywords:* Dynamic model; Heat and mass transfer; Pilot scale; Solar thermal energy; Vacuum membrane distillation

### 1. Introduction and literature review

Potable water and conventional energy are scarce sources in many places especially in arid and remote areas. Insufficient natural sources in remote rural areas along with low infrastructure are problems which will be aggravated dramatically in the future. Methods of removing salt from the sea and brackish waters have been studied, and industrial scale desalination plants have been developed for big cities to become more efficient. The reason is that the desalination techniques are high energy consuming and recommended to be supplied by renewable sources of energy [1]. Stand-alone desalination systems coupled

with solar energy are a possible solution for remote and isolated communities.

In total, there are 26 possible combinations of desalination techniques by various renewable energy technologies [2]. Stand-alone solar still is a common thermally driven desalination process for its simple set-up. However, its thermal efficiency is very low due to its large specific collector area [3]. Desalination techniques are classified into thermal, membrane and hybrid processes [4]. Physical liquid-gas phase transformation is the feature of the thermal processes such as multi-effect distillation (MED) and multi-stage flash (MSF). Separation technology is involved in the membrane process such as reverse osmosis (RO) and electro dialysis. The hybrid process involves both membrane and thermal technologies such as membrane distillation (MD). MSF

\*Corresponding author.

and RO are the advanced processes commercially available. However, those processes are faced with drawbacks such as intensive heat or high pressure demand, pollutants and undesired emissions generation, scaling and fouling problems, membrane cost and its durability [4]. A suitable desalination technology must respond to health risks, territorial and environmental implications despite the economic efficiency term.

MD yields highly purified permeate water through a hybrid membrane-evaporative process, and reduce the investment and maintenance costs [3,5]. The pressure difference across the membrane is the driving force in MD. Various MD configurations such as direct contact membrane distillation (DCMD), air gap membrane distillation (AGMD), sweeping gas membrane distillation (SGMD) and vacuum membrane distillation (VMD) perform this stream in different methods [6]. The suitable processes for desalination purpose are DCMD, AGMD and VMD [7,8]. The efficiency of DCMD, SGMD and VMD were compared, using a PVDF hollow fiber membrane for desalination of salt solution [9]. The highest flux was achieved by the VMD process. Despite attractive features of VMD, especially coupling to low-grade sources of energy, the commercialization requires research on new membrane development to overcome the low permeate flux and wetting problems [4].

In VMD, a hot feed solution is passed over a micro-porous hydrophobic membrane, and low pressure is applied on the permeate side. Water evaporates and passes through the pores via vapor pressure difference across the membrane. The steam is condensed on the permeate side between the membrane module and a vacuum pump. The benefits of the VMD compared with other common separation processes are as follows: complete rejection of ions, macromolecules, colloids, cells and other non-volatiles; lower operating temperatures than conventional distillation and other MD methods; lower operating pressures than pressure-driven membrane separation processes; reduced level of fouling and chemical interaction between membrane and solution; reduced installation area compared with conventional distillation processes. In this way, recent reviews state that the VMD process can successfully be carried out using alternative energy sources such as freely available solar energy [10–15]. The energy source can be harvested with a solar collector and/or photovoltaic (PV) panel or a photovoltaic thermal (PVT) panel to provide both electrical and thermal energy for a VMD system.

Low operational and maintenance costs are the benefits of solar desalination systems, but their major drawback is their low thermal efficiencies [16]. More improvements through the performance were taken into consideration in recent advances for developing a very efficient energy recovery system. It was shown that the specific energy of a desalination unit with RO has been reduced to a value near 1.8 kWh m<sup>-3</sup> [17]. This system utilized high-permeability SWRO membrane elements on a controlled pilot-scale system with 50% recovery. Although for thermal desalination systems the energy consumption varies widely, the variation of the energy consumption of the tested MD methods is between 68.8 and 499.1 kWhm<sup>-3</sup> [18]. An appropriate method of analysis is required to compare the performances. The efficiency of the system in terms of solar

energy incident, thermal energy consumption and the permeate water production has to be evaluated. Gained output ratio (GOR) and thermal recovery ratio (TRR) are significant performance parameters for the assessment of thermal desalination processes [4]. The ratio of the latent heat of evaporation and the input energy to the system defines GOR as follows:

$$\text{GOR} = \frac{H_v J A_m}{\dot{m}_s C_p (T_{m1} - T_{m2})} \quad (1)$$

where  $H_v$  (Jkg<sup>-1</sup>) is specific enthalpy of vaporization,  $J$  (kgm<sup>-2</sup>h<sup>-1</sup>) is the permeate flux,  $A_m$  (m<sup>2</sup>) is the membrane area,  $\dot{m}_s$  (kg h<sup>-1</sup>) is the solar collector mass flow-rate,  $C_p$  (Jkg<sup>-1</sup>K<sup>-1</sup>) is the feed specific heat and  $T_{m1}$  and  $T_{m2}$  (K) are the feed temperatures at the membrane inlet and outlet. Overall, efficiency of a solar based desalination system is determined by the thermal energy required for distillation to the total thermal energy input:

$$\text{TRR} = \frac{H_v J A_m}{G_t A_s} \quad (2)$$

where  $G_t$  (Wm<sup>-2</sup>) is the global solar irradiance and  $A_s$  (m<sup>2</sup>) is the solar collector area.

Integrated desalination systems, solar powered processes, new membrane technologies and different methods of feed water circulation have been incorporated in energy recovery studies for desalination purposes [3,19–23]. Coupling solar energy with MD was the interest of researchers to simultaneously solve the problems of energy and water resources. A solar-powered AGMD unit has been constructed and tested using a spiral-wound membrane module [24]. A large reduction in the permeate flux has been reported due to the additional mass transfer resistance created by the air gap. The feasibility and the features of a solar powered AGMD over other desalination processes have been studied [19]. The PV and thermally driven small-scale, stand-alone AGMD experiments carried out with promising results using a spiral-wound module with an effective membrane area of 10 m<sup>2</sup>. The maximum production rate of the unit reached 120 Ld<sup>-1</sup> with a permeate electrical conductivity of less than 5 µScm<sup>-1</sup>. The earliest simulation results on a solar driven AGMD with a thermal collector area less than 6 m<sup>2</sup> and without heat storage showed that between 120 and 160 L<sup>-1</sup> of water distills during a day in the summer [3]. A larger system consisted of two loops has been employed for desalination of the Red Sea water using a titanium corrosion resistant heat exchanger [20]. Parallel configuration has been performed with four spiral wound membrane modules. Production rate of water and energy requirements ranged between 600–800 Ld<sup>-1</sup> and 200–250 kWhm<sup>-3</sup>, respectively. The system was benefited by 72 m<sup>2</sup> thermal collector area and 40 m<sup>2</sup> total membrane area. The calculated GOR and energy consumption were 5.5 and 117 kWhm<sup>-3</sup>, respectively, for a volume flow of 350 Lh<sup>-1</sup> at an evaporator inlet temperature of 75°C. In addition, simulations have predicted thermal and electrical energy consumption fluctuated from 5 to 12 kWhm<sup>-3</sup> and 0.6 to 1.5 kWhm<sup>-3</sup>, respectively, for a system without energy recovery [25]. Two different configurations of membrane

modules have been evaluated using the combination of AGMD and solar collector [1]. Performance of the multi-stage formation was proven to be better than the strategy of one compact module with greater area. In this AGMD system, the parametric study results show that higher feed temperature and effective membrane length had a significant effect in lowering the cost while higher feed flow rate, higher air gap width and feed channel depths resulted in increased water production cost [26].

There are two different configurations for DCMD powered by solar energy: Feed water can be heated directly inside collectors or by means of an intermediate heat exchanger [27]. One of the earliest solar-powered DCMD systems distilled 17 Ld<sup>-1</sup> per square meter of collector area resulting in specific energy consumption of 55.6 kWhm<sup>-3</sup> [28]. A flat plate module and a 12 m<sup>2</sup> field of vacuum tube thermal collectors were used in this plant. A combined system studied by Suárez et al. (2010) showed that, permeate water distills 1.6 Ld<sup>-1</sup> with membrane areas ranging from 10 to 13 cm<sup>2</sup> per square meter of salt gradient solar ponds (SGSP). This study was benefitted by the coupled DCMD with SGSP [29]. A novel energy recovery unit has been simulated in a solar-assisted DCMD system for production of fresh water from seawater [5]. This concept reduces temperature fluctuations of the feed water by storing the collected energy during solar-peak hours and employing heat from the permeate and brine streams to the feed seawater. The maximum permeate flux of 51.1 kgm<sup>-2</sup>h<sup>-1</sup> was calculated at 0.2 m length of the module with the hot and cold stream temperatures of 80°C and 30°C and flow rates of 6 Lmin<sup>-1</sup>. For production capacity of 31 m<sup>3</sup>d<sup>-1</sup>, about 160 m<sup>3</sup> seawater storage tanks, 3,360 m<sup>2</sup> of evacuated-tube collectors and 50 membrane modules were incorporated. The modules consist of a porous hydrophobic membrane assembled together in a shell-and-tube module. Evaporation from solar ponds and variation of the temperature along the entire membrane is drawback of this system. It has been shown that DCMD is an effective process compared with AGMD and VMD considering heat recovery despite the conductive heat losses from the feed to the permeate side [30].

The performance of a solar-heated hollow fiber VMD system for potable water production from underground water has been described [15]. This system contains four major components: a solar energy collector; a hollow fiber membrane module; a condenser; and centrifugal vacuum pumps. The experimental results reported the largest permeate flux of 32.2 kgm<sup>-2</sup>h<sup>-1</sup> in 16th October at 1:00 pm via 500 hollow fiber membrane modules with 0.1 µm pore size and 0.09 m<sup>2</sup> area per module. The area of the solar collector is 8 m<sup>2</sup>. The electro conductivity was reduced from more than 230 mScm<sup>-1</sup> to less than 4 µScm<sup>-1</sup>. There are no calculations reported for the GOR and TRR, and the energy required for passing cool water through the condenser is not described. The combination of VMD with solar collector or SGSP was undertaken for the simulation study [8]. The results showed that the combined VMD-SGSP system will increase concentration and temperature polarization phenomena at the membrane feed solution interface and will result in flux reduction. However, it was concluded that the VMD coupled with a solar collector is more practical due to the ability of increasing the feed water temperature with thermal energy. The highest flux of 140 Lm<sup>-2</sup>h<sup>-1</sup>

could be obtained through a vacuum pressure of 0.5 kPa. The energy recovery was not studied in this work. The optimal operating conditions for an energetic performance of the pilot plant solar powered VMD was investigated [31]. The designed installation is based on the application of only solar power as an energy source to produce about 210 kg of water per day. Flat plate collectors were selected due to a technical-economic study of different types of solar collectors. The simulation study concluded that the total collector area of 70 m<sup>2</sup>, 16 PV panels, 8 batteries and 806 hollow fiber module with 4 m<sup>2</sup> area per module are required to produce from 8.75 to 17.5 Lm<sup>-2</sup>h<sup>-1</sup> of permeate water. The experimental study of this plant is still in progress. A comprehensive review and assessment of established solar-powered membrane distillation (SP-MD) systems reported that only one solar powered VMD, and two solar powered DCMD systems have been evaluated till 2012 while the other studies have been focused on the AGMD type [32]. Low GOR values ranging from 0.3 to 6.0 were reported for the 16 studied experimental works. The calculated GOR for solar powered VMD was 0.85 with thermal energy consumption of 7,850 kWhm<sup>-3</sup>. The high value of energy consumption is due to the use of 0.09 m<sup>2</sup> membrane area.

Despite many benefits of a VMD system, very few experimental systems have been developed and compared with solar RO and solar desalination, and such systems have not been commercialized. Furthermore, modeling and optimization of solar powered MD systems are less explored. Despite most of the previous studies associated with technical and economic feasibility assessment and/or prediction performance derived from a steady-state condition of solar powered MD, the objectives of this study are to design an efficient solar powered vacuum membrane distillation (SVMD) system with heat recovery, and to develop a dynamic mathematical model based on an unsteady-state process for the prediction of system performance. Therefore, this research provides:

- The design and construction of a solar powered (using sun tracker for both PV panel and solar collector) coupled with VMD (containing two loops to extract heat from condensation unit).
- Mathematical modeling of a heat and/or mass transfer process through the solar collector, membrane module and condensation unit.
- Numeric solution of the model using a simulation computer program.
- Implementation and validation of the model by comparison with experimental data as well as its sensitivity analysis.

## 2. Solar membrane distillation process

A modified VMD process coupled with solar energy was used for the purpose of this work. A schematic diagram of the solar based VMD system (SVMD) is shown in Fig. 1. The system comprises of two PV panels, a thermal collector, a condenser unit and a hollow fiber membrane module. The PV panels provide electrical energy for the pumps. The thermal collector supplies the hot feed water for the membrane module. SVMD consists of two separate

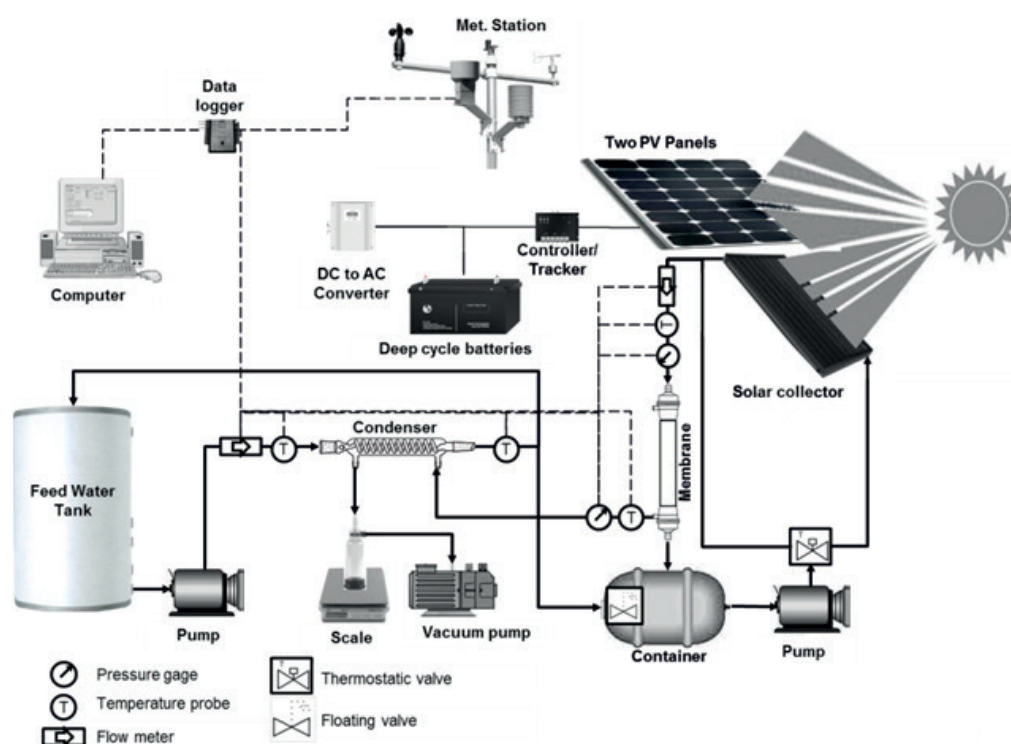


Fig. 1. Solar powered vacuum membrane distillation system.

loops and a distillate channel. The feed solution is passed through the first loop from the condenser inlet to a storage container which is designed to increase the temperature for energy savings. The feed water is then heated in the second loop via the solar collector and directed along to the membrane module. The VMD water circuit is made of thermally insulated tubes. Permeate water is gained in the distillate channel while vapor is extracted by the means of pressure difference. For that reason, a hydrophobic membrane is used to create an interface between the hot feed solution and the vapor on the permeate side. A variety of transducers and sensors were embedded to monitor the weather conditions, system performance and water quality.

### 2.1. VMD configuration

The SVMD system has two major loops as shown in Fig. 1. A digitally controlled Masterflex peristaltic pump circulates feed solution from the water tank. Feed water is heated up when passed via the condenser. Feed water then fills the container until the level of water rises to the pre-set height. A floating valve shifts the stream of the feed water from the container to the feed tank. Another peristaltic pump in the second loop adjusts the flow rate of feed water through the solar collector followed by the membrane. Temperature of the feed water reaches the ultimate level at the outlet of the solar collector in the second loop. A three-way thermostatic valve bypasses the solar collector when feed water reaches the ultimate temperature (65°C). The valve sensor reads the temperature of the container and leads water directly to the membrane if necessary. It is important to ensure that the recirculation hose at the membrane outlet

remains above the membrane level so that the membrane module remains full at all times. The evaporation process takes place in a hollow fiber membrane, and the residue of hot feed water is directed afterwards into the container. An incorporated ball valve onto the N820-KNF laboratory vacuum pump (Javac) is used to apply and release vacuum pressure. The vacuum pump withdraws vapor into the condenser on the permeate side of the membrane by means of applying pressure lower than the saturation pressure of vaporization. A glassware condensation column containing three cavities of spiral tube, cold water cylinder and condensed vapor tunnel is employed in order to increase the efficiency of such a system compared with the one with external condenser working with cold water source.

### 2.2. Membrane module

So far, commercially available hydrophobic membranes such as polypropylene (PP) polytetrafluoroethylene (PTFE) or polyvinylidene fluoride (PVDF) were studied for MD. The hydrophobic nature depends on pore size, membrane materials and liquid characteristics. It is possible for water to intrude into the pores as a result of applying higher pressure difference than the liquid entry pressure (LEP). Higher LEP is achieved with higher hydrophobicity and smaller pore size; however, in turn the permeability of the membrane will be reduced considering no change in the porosity, thickness and pore tortuosity. Hydrophobic PTFE membranes enjoy high LEP followed by PVDF and PP membranes. Hence, a commercially available micro-porous membrane made of PP in capillary form which is hydrophobic was selected due to the rate of flux and used in the VMD experiments. The hollow

fiber MD020CP2N (MICRODYN) module with 40 capillaries has the surface area and pore diameter of  $0.1 \text{ m}^2$  and  $0.2 \mu\text{m}$ , respectively. The benefit of hollow fiber membrane to flat type is the higher ratio of the membrane surface area to module volume. The LEP of the employed membrane is 140 kPa as suggested by the manufacturer. The PP module is 65 mm in thickness and 0.47 m in length.

### 2.3. Solar photovoltaic and collector technologies

The VMD process couples solar collectors and PV panels to provide thermal and electrical energy. The PV cells convert solar irradiance into an electric current. Crystalline silicon type of PV is a dominant technology with the conversion efficiency of about 16% [33]. Two SPR-210-SunPower panels designed for use in on-grid residential and commercial systems were embedded in this study. The panels offering a total area of  $2.48 \text{ m}^2$  support ultimate 420 W power at 48 VDC into the solar regulator to load the requirements of the batteries. The system includes two deep cycle batteries (60AH 12V AGM, Aussie Batteries and Solar) to store and produce energy for the pumps. In order to increase the efficiency of such system, a Lorentz ETRACK controller tracks the sun along with the PV panels mounted on this tracker system. In regard to the local meteorological conditions, a sun-tracking unit was adjusted for the east-west track. The best orientation for the altitude angle to the north or south is the latitude of the location.

Absorb and transfer solar irradiance into thermal energy is achieved in solar stills, collectors, or solar ponds. Solar collectors are different in glazing type, selectivity and absorber material. The efficiency of a collector is influenced by inclination and orientation. Three configurations of collectors are developed such as the parabolic-trough, compound parabolic and the flat plate collector. Although, the first one is known as a tracking collector, in this research, a plate collector is attached to the solar panel to be benefitted by the tracking advantage. The solar collector adopted in this study consists of an area of  $1.5 \text{ m}^2$ . Insulation has been used for the entrance and exit hoses. Moreover, a local meteorological station was mounted in a trailer in order to monitor and investigate the

influence of parameters such as solar irradiance, ambient temperature, humidity and wind speed.

### 2.4. Monitored parameters in SVMD

Operating parameters were measured for the two temperature control loops. Temperature gradient across the condenser was monitored by two temperature sensors. The outlet temperature of the thermal collector and the temperature at the membrane inlet were also measured. A temperature sensor on the permeate side of the membrane read the vapor temperature, separately. Two flow-meters in each loop gauged the flow rate of cold and hot feed streams. As shown in Fig. 1, a pressure probe measured the vacuum pressure on the permeate side of the membrane. The cumulative weight of the permeate trap was monitored by a BA4100 Sartorius balance ( $\pm 0.1 \text{ g}$ ). All dynamic measurements, including temperature, flow-rate, pressure and weight of water, were recorded using a data acquisition system. On the other hand, climate parameters such as temperature, humidity, solar irradiance, wind speed and direction were also transferred to the data logger.

The cold feed stream was circulated at  $250 \text{ mL min}^{-1}$  flow rate for efficient condensing as well as providing higher temperature feed flow to the collector. The hot stream flow rate was adjusted manually for  $500 \text{ mL min}^{-1}$ . Moreover, experiments were carried out under high vacuum pressure at 6 kPa.

## 3. Model development

Thermodynamic analysis has been performed to investigate in detail the thermal performance of the SVMD system. Heat transport mechanisms in SVMD mainly consist of the heat transported across the solar collector, heat and mass transported across the membrane, the heat transferred in the condenser, the latent heat of condensation of the produced vapor and the heat losses to the surroundings. The mass and energy balance is established for the system as shown in Fig. 2. The external heat from the solar collector,

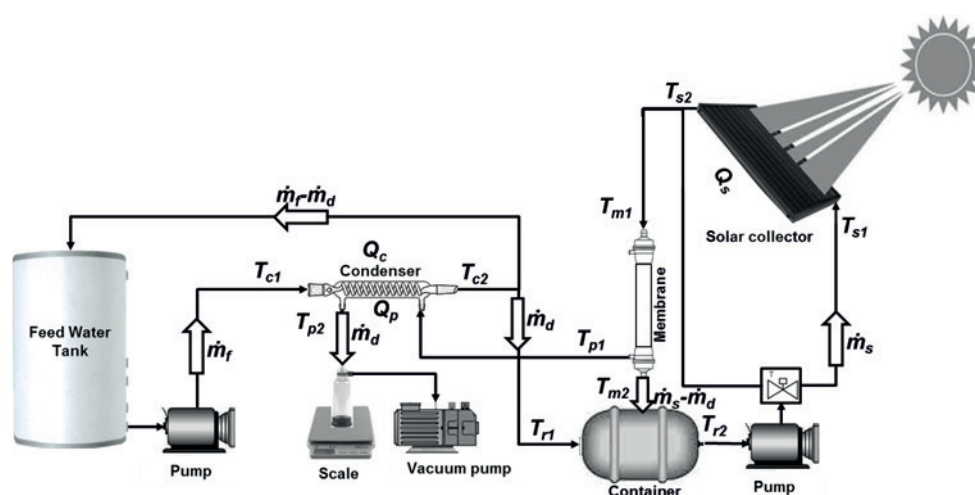


Fig. 2. Heat and mass transfer in the SVMD system.

$Q_s$ , is modeled through the available data of solar irradiance for specific location. Feed water is warmed up through the condenser where  $Q_c$  is condenser heat. The enthalpy of the distillate within the condenser is named  $Q_p$ . Finally,  $Q_{loss}$  accounts for the heat losses to the surroundings. The heat and mass transfer analysis of the SVM system requires two assumptions: The feed water tank volume is considerably great so the recirculated mass flow rate ( $\dot{m}_f - \dot{m}_d$ ) has no effect on the temperature of the inside tank. However, the temperature of feed water ( $T_{c1}$ ) depends on the ambient temperature ( $T_a$ ). In regard to the total loss of heat considered in this system, the following temperature values are assumed to be equivalent: temperature at condenser outlet and container inlet ( $T_{c2} = T_{r1}$ ); temperature at container outlet and solar collector inlet ( $T_{r2} = T_{s1}$ ); temperature at solar collector outlet and membrane inlet ( $T_{s2} = T_{m1}$ ); temperature at permeate side of the membrane and condensed trap ( $T_{p1} = T_{p2}$ ), since it is assumed that the enthalpy of condensation is more considerable in comparison with the heat transfer by convection. Mass flow rate from the feed tank ( $\dot{m}_f$ ) will be divided into two parts after the condenser. The recirculated mass flow ( $\dot{m}_f - \dot{m}_d$ ) is returned to the feed tank and the same distillate mass flow ( $\dot{m}_d$ ) will head to the container. The floating valve used in the container accepts the same mass flow which is distilled and extracted on the permeate side of the membrane. It shows the relationship between mass transfers through the first and second loops. In addition, the mass flow through the solar collector ( $\dot{m}_s$ ) is directed to the membrane and divided into two streams. The recalculated mass to the container ( $\dot{m}_s - \dot{m}_d$ ) is reduced by the rate of permeate flux. The relevant heat and mass transfer equations are given in the following sections followed by a solution method. Thermal equilibrium in the container via the mass flow rates at the two inlets and outlet is given by:

$$\dot{m}_d T_{r1} + (\dot{m}_s - \dot{m}_d) T_{m2} + \frac{Q_{loss}}{C_p} = \dot{m}_s T_{r2} \quad (3)$$

### 3.1. Solar radiation and ambient temperature

A two-dimensional empirical model visualized time and month is developed to quantify dynamic behavior of solar energy. In this regard, solar irradiance data of three different geographical locations in Australia: Sydney (33.86° S, 151.21° E), Perth (31.95° S, 115.86° E) and Darwin (12.45° S, 130.83° E) were obtained from Australian and New Zealand Solar Energy Society (ANZSES) [34]. The proposed model is applied to the solar irradiance data of these sites to validate the parameters. The exponential model similar to the amplitude version of Gaussian peak function was employed for the hourly solar irradiance function, and the correlated parameters. The general form of an exponential function for monthly average hourly solar irradiance ( $G_t$ ) for Sydney is given in Eq. (4):

$$G_t = C + Ae^{\left[-0.5 \left( \frac{t-12}{2.925} \right)^2\right]} \quad (4)$$

where  $t$  is the time and the parameters  $C$  and  $A$  are related to the tendency and height of the peak function, respectively.

These parameters have to be determined for each location, separately. The average of solar irradiance data observed for each month implies that these parameters are not constant, and their variations are not linear. An amplitude version of Gaussian peak function predicts the trend of these parameters for each month during the course of a year. The developed functions of the two parameters  $C$  and  $A$  for Sydney were expressed as follows:

$$C = -82.8 + 53.6e^{\left[-0.5 \left( \frac{m-6}{1.54} \right)^2\right]} \quad (5)$$

$$A = 934.5 - 232.4e^{\left[-0.5 \left( \frac{m-5.79}{1.49} \right)^2\right]} \quad (6)$$

The parameter  $m$  in this function is varying by month. Solar irradiance on the tilted surface with east-west tracking is graphed in Fig. 3(a) using Eq. (4). Accumulated data of the ambient temperature leads to determine the feed water tank relationship. Fig. 3(b) shows the monthly average hourly ambient temperature obtained from the ANZSES

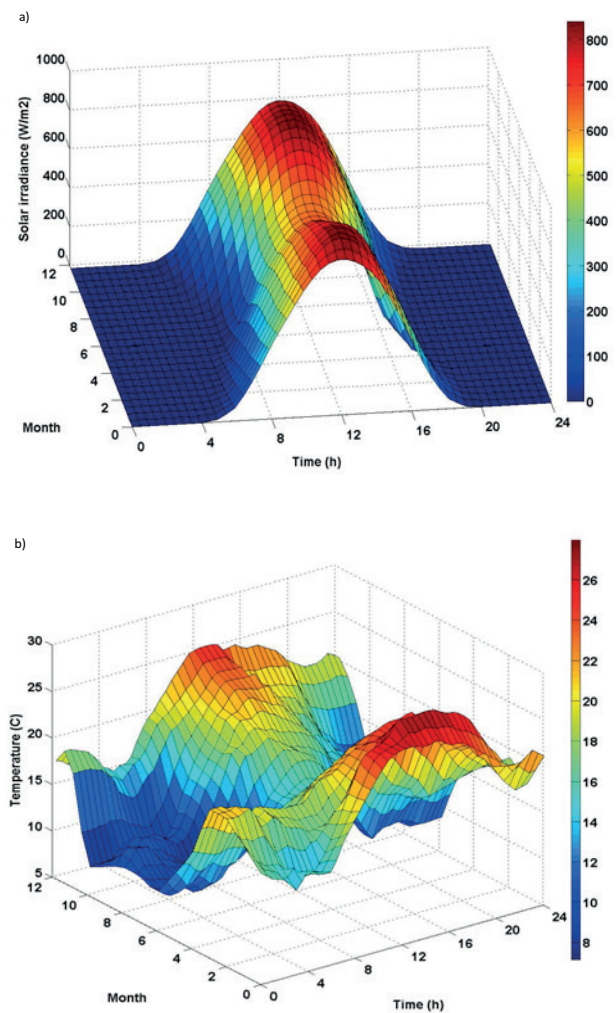


Fig. 3. (a) The monthly average hourly solar irradiance and (b) the monthly average hourly ambient temperature (°C) for Sydney.

data. From Fig. 3, it can be seen that the maximum monthly average hourly ambient temperature and the irradiance are approximately 28°C that occurs in January and about 850 W m<sup>-2</sup> in October, respectively.

### 3.2. Heat transfer in solar collector

Based on the monthly average hourly global irradiance on a tilted solar collector, the transported energy for heating purposes is calculated by means of transmissivity coefficient. The energy obtained from the solar collector ( $Q_s$ ) is defined as:

$$Q_s = \eta A_s G_t + K_h W A_s \left( T_a - \frac{(T_{s1} + T_{s2})}{2} \right) \quad (7)$$

where  $A_s$  (m<sup>2</sup>) represents the area of the solar collector,  $\eta(-)$  is the coefficient of transmissivity,  $K_h$  (W.s m<sup>3</sup>K) is the coefficient of heat transfer, and  $W$  (m s) is wind speed at 3 m above the ground. An established meteorological station collects solar irradiance, ambient temperature and wind speed data in order to determine the accuracy of transferred energy by Eq. (7). The absorbent material plays an important role in the level of captured energy. The energy absorbed is not entirely transferred to the fluid, due to a part of dissipation as heat loss from the absorber. Obtained experimental values from the performance of the SVM system defines coefficient of transmissivity as the ratio of the efficient energy delivered to the total solar irradiance as

$$\eta = \frac{\dot{m}_s C_p (T_{s2} - T_{s1}) - K_h W A_s (T_a - \frac{(T_{s1} + T_{s2})}{2})}{A_s G_t} \quad (8)$$

It is assumed that the flow through the solar collector ( $\dot{m}_s$ ) reaches to the temperature which is the same as the inlet temperature of the membrane.

### 3.3. Heat and mass transfer across the membrane

The heat transfer mechanism across the membrane can be divided into two regions. Feed and membrane boundary layers are series of resistances in VMD. Convective and conductive heat transfers are considered in this research across the membrane module. In regard to the analogy between electrical and thermal conduction process at steady state condition, the heat transfer through the membrane can be expressed as follows:

$$Q = Q_m \quad (9)$$

where  $Q$  and  $Q_m$  are heat transfer through the feed and membrane boundary layers, respectively. Convection ( $Q^{conv}$ ) and heat transferred by mass transfer ( $Q^M$ ) in the feed boundary layer are represented as follows:

$$Q_f = Q^{conv} + Q^M = A_m h_f (T_{m1} - T_f^m) + \dot{m}_d H_f^f \quad (10)$$

Conduction ( $Q^{cond}$ ) and heat transfer by water vapor stream through the membrane ( $Q_m^M$ ) are given as follows:

$$Q_m = Q_m^{cond} + Q_m^M = A_m h_m (T_f^m - T_{p1}) + \dot{m}_d H_v^m \quad (11)$$

where  $T_f^m$  is temperature at membrane surface and  $T_{m1}$  and  $T_{p1}$  are the feed solution and permeate vapor temperatures. In the cited equations,  $h_f$  and  $h_m$  (Wm<sup>-2</sup>K<sup>-1</sup>) represent the corresponding heat transfer coefficients in feed and membrane boundary layer, respectively. The enthalpy of feed ( $H_f^f$ ) and vapor ( $H_v^m$ ) are determined at average temperature of fluid in each region. Membrane heat transfer coefficient ( $h_m$ ) can be derived from the thermal conductivity of the membrane ( $k_m$ ). Thermal conductivity of a hydrophobic porous membrane depends on polymer conductivity ( $k_p$ ), vapor conductivity ( $k_v$ ) and membrane thickness ( $\delta$ ). Membrane porosity ( $\epsilon$ ) determines the ratio of the solid and gas conductivities.

$$h_m = \frac{k_m}{\delta} = \frac{k_v \epsilon + k_p (1 - \epsilon)}{\delta} \quad (12)$$

The heat transferred by mass transportation in the feed boundary is negligible compared with the convection transfer type [35]. Therefore, the overall heat transfer coefficient ( $h_o$ ) of the membrane can be obtained by Eq. (13):

$$h_o = \left( \frac{1}{h_f} + \frac{1}{h_m + \frac{\dot{m}_d H_v^m}{T_f^m - T_{p1}}} \right)^{-1} \quad (13)$$

Boundary layer heat transfer coefficient ( $h_f$ ) can be estimated from empirical correlations. In the VMD process, dimensionless numbers with correction factors were used to determine heat transfer coefficients. The heat transfer coefficient for laminar flow in circular tubes was estimated [36] using Nusselt number as Eq. (14):

$$\frac{hd}{k_T} = Nu = 3.66 + \frac{0.067 G_z}{1 + 0.04 G_z^{2/3}} \quad (14)$$

where  $G_z$  is Graetz number determined as follows:

$$G_z = \frac{\dot{m} c_p}{k_i L} \quad (15)$$

where  $\dot{m}$  is mass flow rate,  $c_p$  is heat capacity,  $L$  is the membrane length and  $k_i$  is thermal conductivity. Furthermore, Qtaishat et al. [35] proposed an empirical correlation for turbulent pipe flow as follows:

$$Nu = 0.027 Re^{0.8} Pr^c \left( \frac{\mu_f}{\mu_m} \right)^{0.14} \quad (16)$$

where  $Re$  is Reynolds number,  $Pr$  is Prandtl number,  $c$  is 0.4 and 0.3 in the case of heating and cooling, respectively, and  $\mu_f$  and  $\mu_m$  are dynamic viscosities of fluid at the bulk and membrane surface, respectively. The dynamic viscosity of fluid at any temperature  $T$  (°C) can be obtained by Andrade correlation [37] as follows:

$$\ln(\mu) = A + B / T \quad (17)$$

where A and B are constants and can be determined experimentally.

In addition, thermodynamic equilibrium is assumed for heat transfer along and across the membrane. This equilibrium explains the equivalent reduction of temperature of water from the inlet to the outlet of the membrane and the heat obtained for the vaporization through the membrane. Heat transfer along the membrane from the inlet to the outlet is correspondent to the enthalpy difference between feed solution at temperature  $T_{m1}$  and vapor at temperature of  $T_{p1}$ . Accordingly, it can be expressed by Eq. (18):

$$(\dot{m}_s - \dot{m}_d)C_p(T_{m1} - T_{m2}) = \dot{m}_d(H_{v,T_{p1}}^m - H_{l,T_{m1}}^f) \quad (18)$$

The concept of vapor flux and heat transfer through a hydrophobic membrane is illustrated by vaporization of the feed solution passed on one side of the membrane. Water molecules in the gaseous vapor state are transported through the micro-porous hydrophobic membrane by applying vacuum pressure on the permeate side of the membrane. Mass transfer mechanism in a VMD process is described by the Kinetic theory of gases. A model or a combination of the Knudsen flow and the viscous flow demonstrate mass transfer in the VMD process. The ratio of mean free path ( $\lambda$ ) of the transported vapor molecules to the diameter of the membrane pores ( $d$ ) provides Knudsen number ( $K_n = \lambda d^{-1}$ ) which can be used as a guideline to determine the accurate mechanism of mass transfer. For a given membrane pore diameter, the Knudsen number is obtained using the estimation of mean free path by Eq. (19) as follows [38]:

$$\lambda = \frac{k_B T}{\sqrt{2\pi P} \sigma^2} \quad (19)$$

where  $k_B$  is Boltzmann constant ( $1.381 \times 10^{-23}$  JK<sup>-1</sup>),  $T$  is the absolute temperature,  $P$  is the mean pressure within the membrane pores and  $\sigma$  is the collision diameter (2.641 Å for water vapor). Molecule-pore wall collisions are likely dominant for a membrane with small pores ( $K_n > 1$ ). Therefore, the Knudsen-flow regime has to be explained by the Knudsen diffusion model expressed in Eq. (20) for vapor passing through small holes in a thin wall [38,39]. The number of molecules passing through a pore is directly proportional to the driving pressure of the gas and inversely to its molecular weight:

$$N_w = \frac{2\varepsilon r}{3\tau} \frac{\Delta P}{R\delta T_f^m} \left( \frac{8RT_f^m}{\pi M_w} \right)^{\frac{1}{2}} \quad (20)$$

where  $\varepsilon$  is the membrane porosity (-),  $r$  is the average of the pores radius (m),  $\tau$  is the membrane tortuosity (-),  $N_w$  is the molar flux (mol m<sup>-2</sup>.s<sup>-1</sup>),  $\Delta P$  (Pa) is the pressure difference between the partial pressure of the solution and the absolute vacuum pressure,  $R$  is the gas constant (8.31 Jmol<sup>-1</sup>K<sup>-1</sup>),  $\delta$  is the membrane thickness (m) and  $M_w$  is the molecular weight of water (18.01528 gmol<sup>-1</sup>). Vapor temperature at the feed side of the membrane is determined via the vapor flow rate using a value for molar flux rate. The mass flow-rate,  $\dot{m}_v$  (kgs<sup>-1</sup>) of vapor through membrane pores is calculated using Eq. (21):

$$\dot{m}_v = N_w A_m M_w \quad (21)$$

where  $A_m$  is the total membrane surface area (m<sup>2</sup>). Since, enthalpy of vapor is larger than water, and the heat transfer coefficient of fluid is dominant to the membrane, the vapor temperature at the feed side of the membrane can be simplified using Eqs. (10) and (11) as follows:

$$T_f^m = T_{m1} - \frac{\dot{m}_v H_{lv}}{h_f A_m} \quad (22)$$

The heat transfer coefficient of feed solution is influenced by the Nusselt Number ( $Nu$ ) which is proportional to the Reynolds Number and Prandtl Number. So the effect of feed-water velocity is considered in the degree of heat loss between the feed water and the feed side of the membrane surface. Feed-water heat transfer coefficient is derived using Eq. (23):

$$h_f = \frac{Nu k_T}{D} \quad (23)$$

where  $D$  is the diameter of fiber at membrane inlet. Pressure difference across the membrane is influenced by the feed side temperature. Antoine's equation expressed in Eq. (24) relates temperature to the water vapor saturation pressure at the liquid-vapor interface [40].

$$P_{sat}(T_f^m) = e^{\left( \frac{23.1964 - \frac{3816.44}{T_f^m - 46.13}}{T_f^m} \right)} \quad (24)$$

The assumption here is the negligible effect of curvature of the liquid-vapor surface compared with the flat surface state. The saturation pressure requires adaptation through the TDS concentration in the feed solution. Partial pressure is expressed by Eq. (25):

$$P_w = x_w a_w P_{sat}(T_f^m) \quad (25)$$

where  $x_w$  is the water mole fraction derived from concentration of salts in water and  $a_w$  is the activity coefficient of water which is explored by Eq. (26) [38]:

$$a_w = 1 - 0.5x_{NaCl} - 10x_{NaCl}^2 \quad (26)$$

where  $x_{NaCl}$  is the sodium chloride (NaCl) mole fraction.

Viscous flow arises where the molecule-molecule collision is dominant for membrane with large pores ( $K_n < 0.01$ ). In this case, Eq. (27) was developed to determine molar flux [12,38]:

$$N_w = \frac{\varepsilon \pi r^4 P_{ave}}{8\mu_f R T_f^m A_m \tau \delta} \Delta P \quad (27)$$

where  $P_{ave}$  is average partial pressure (Pa).

Both molecule-molecule and molecule-pore wall collisions occur in the transition region ( $0.01 < K_n < 1$ ). In addition, surface diffusion is negligible for pore size higher than 0.02  $\mu$ m due to the fact that the pore area is significantly larger than the surface diffusion area. The Dusty-Gas model was developed in the transition region to describe the VMD

performance [41]. Eq. (28) is based on the assumption of both molecule-pore wall and molecule-molecule interactions [6].

$$N_w = \frac{\Delta P}{\delta RT_f^m} \left[ \frac{2\epsilon r}{3\tau} \left( \frac{8RT_f^m}{\pi M_w} \right)^{\frac{1}{2}} + \frac{\epsilon r^2 P_{ave}}{8\tau \mu_f} \right] \quad (28)$$

The presented models predict flux response to changes in temperature, pressure, flow rate and feed solution salinity for a specific membrane. In this research, the Knudsen number calculated from Eq. (19) for MD020CP2N membrane was in the range of 0.01 to 1, so Knudsen-viscous flow is the dominant phenomenon for mass transfer through a porous media.

### 3.4. Heat transfer in condenser

The important concept in the study of condensation unit for the VMD process is to bring the vapor to a cooler surface. Heat transfer during this can be modeled using a simple mathematical equation. Water vapor will be condensed when subjected to a temperature below its saturation temperature,  $T_{sat}$ , at a certain pressure,  $P_{sat}$ . This has been achieved by passing the vapor into contact with a solid surface with a lower temperature. Although both condensation and temperature variation of the permeate vapor are performed through specific glassware condenser as shown in Fig. 2, the enthalpy of condensation is considered as a major heat transfer term. The enthalpy of the distillate ( $Q_p$ ) is equivalent to the condenser heat transfer ( $Q_c$ ) as follows:

$$\dot{m}_d H_{lv} = \dot{m}_f C_p (T_{c2} - T_{c1}) \quad (29)$$

The mass flow of vapor through the condenser is determined by the membrane mass transfer equation. The enthalpy of condensation is derived from experimental temperature of the permeate liquid in the trap at the assigned constant pressure.

### 3.5. Resolution method

There are several ways to solve simultaneous sets of equations and variables. In this study, the constant parameters were first defined, and the variables were introduced. The variables were then determined by the presented equations. The equations were divided into two sections: derived energy from solar (Eqs. (4)–(7)) and flux calculation (Eqs. (9)–(29)). Input energy was calculated for a specific date. Then, energy losses were determined using a set of experimental data. The results from energy calculation were incorporated with the experimental observation of the ambient temperature as an input for the solution of the permeate flux equation set. All the equations were developed on the MATLAB software, and desired graphs were plotted.

## 4. Results and discussion

The discussion focuses on the performance of the small scale SVMD system as well as the validation and verification of the proposed model followed by the effect of operating

conditions on the permeate flux rate. The calculated range of GOR for the proposed system is 0.34–2.09. It has to be mentioned that the membrane area of 0.1 m<sup>2</sup> has been used. The permeate flow rate can be increased by raising the membrane area and maintaining the vacuum pressure constant. The GOR of this system is in the range of the studied paper and has this opportunity for enhancement. The predicted performance by the developed model is applied for a whole year with and without heat loss effect. The model is also compared with the experimental data. All relevant temperatures, flow rates, flux, pressures and meteorological conditions were monitored for 25 days during a 2-month period. The evolution of the distillate flow vs. time is obtained by both experimental measurements and theoretical calculations. The results mainly concern the variation of different irradiances, and also show the effect of ambient temperature and wind speed over time. Furthermore, the sensitivity analysis of the model is carried out by variation of operating parameters as well as membrane characteristics. Finally, the results achieved by desalination of brackish water are discussed.

### 4.1. Model verification

Five series of experiments were conducted to determine the coefficient of transmissivity as well as the loss of heat. Transmissivity coefficient derived from Eq. (8) specifies the net transported heat from the collector. A coefficient of 0.15 has been calculated for the current solar system. The heat loss was calculated as a function of energy obtained from the solar collector ( $Q_g$ ). The heat loss equation is determined by a function of time multiplied by the term  $Q_s$ . Simulated data are plotted for two cases: with and without heat loss. The permeate flux curve increases gradually at the beginning of the day and reached a maximum depending on the feed-water temperature and then it decreases gradually. The effect of solar irradiance is significant to achieve the highest feed temperature in comparison with the ambient temperature.

The performed simulation illustrated that by ignoring heat losses, a maximum 10 to 14 Lm<sup>-2</sup>h<sup>-1</sup> flux rate is possible as shown in Fig. 4(a). The results are outstanding due to no existing limitation for maximum temperature. The flux rate increases in the summer time from a monthly view and reaches the maximum between 12 and 2 p.m. each day. The production rate increases from 5 to 7 L from winter to summer with the existing MD020CP2N membrane. The equation of heat loss was incorporated to the simulation to predict the realistic performance of this system. The results are shown in Fig. 4(b). The monthly maximum hourly simulated rate of flux varies between 4.7 and 6.5 Lm<sup>-2</sup>h<sup>-1</sup> at 12 p.m. The simulated results also show that flux increases starting at 8 a.m. and reaches zero again at 4 p.m. in the summer time. The daily clean water production using the MD020CP2N membrane with 0.1 m<sup>2</sup> area varies from 2.4 to 3.2 L from winter to summer.

The simulation was developed to predict the hourly rate of flux each day. Collected data from the meteorological station such as solar irradiance, ambient temperature and wind speed were imported instead of using the monthly average hourly data observed for a year. The time step of 6 min was considered for the calculation of temperature at

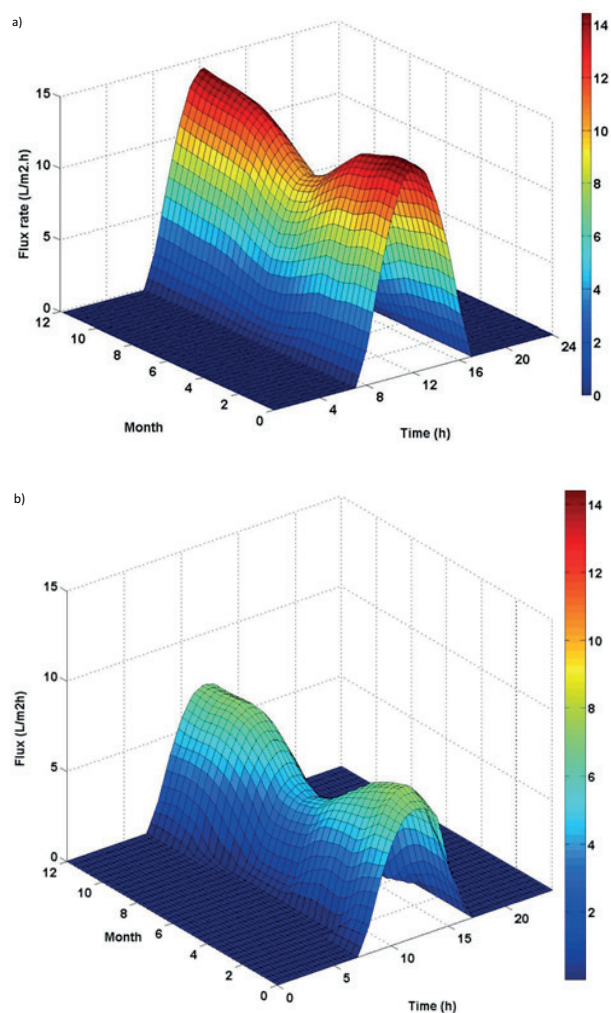


Fig. 4. (a) The monthly average hourly simulated rate of flux without heat loss and (b) with heat loss.

the solar thermal outlet. The various graphs in Fig. 5 represent the typical daily measurements of experimental flux, solar irradiance, electrical conductivity of the permeate, ambient temperature, wind speed, relative humidity and simulated flux for selected dates in December 2013 and January 2014. The simulation study successfully predicted the permeate flux rate except for the points where the solar irradiance changes suddenly.

The gradual increase and decrease of the solar irradiance is observed on the 11th and 17th December and 6th January results in steadily increase and decrease of the flux rate. Solar irradiance increases feed-water temperature using the thermal collector and directly influences the rate of flux. Wind speed is a function that plays with the value of the energy loss. Highest permeate flux was achieved at 1.20 p.m. on 10th December when the solar irradiance reached its maximum value. The ambient temperature was between 35°C and 40°C at that time along with low humidity and wind speed. Accordingly, maximum distillate production was registered at maximum irradiance and ambient temperature. The rate of flux decreases due to the sharp reduction of solar irradiance after 2 p.m. The increase of

irradiance before 3 p.m. was also the reason of flux rate rise at that time. There was no significant change in temperature and humidity of 10th December.

It has to be noted that the system was located in a relatively shaded area where availability of direct solar input was limited. The lowest rate of flux was observed on 28th January about 2.1 Lm<sup>-2</sup>h<sup>-1</sup>. Solar irradiance variation followed by ambient temperature below 30°C and high humidity expressively explains the small rate of flux. The same performance has been observed on 8th January; however, the morning and afternoon irradiance were not sufficient to increase the water temperature to the required level. The effect of rapid changes of irradiance along with temperature and humidity due to the cloud cover is noticed on 2nd and 5th December. However, the simulated model has slightly different from the experimental results. On 13th December, experimental flux showed the effect of radiation whereby it achieved the highest level of flux rate between 1.15 and 1.45 p.m. The increase for the simulated model was slight due to the effect of ambient temperature and humidity as well as wind speed. For smooth results of ambient temperatures and humidity as well as solar irradiance on 18th December afternoon, the simulated model predicts well the trend of the flux decline. In addition, from all experimental achievements, it can be concluded that there is a remarkable improvement in distillate production at high ambient temperatures where the solar irradiance is similarly changed. For all performed tests, electro-conductivity varied between 0.6 and 1.6 μScm<sup>-1</sup> that shows a high quality of the permeate water. The variation of electro-conductivity is due to the signals monitored by the data logger.

#### 4.2. Influence of feed temperature

The series of experiments carried out by the SVM system also depicted that there are clear differences between the distribution of the permeate flux results. This is attributed to the variation of feed-water temperature analyzed in the mass and heat transfer mechanisms. Permeate flux reached maximum value between 12 and 2 p.m. depending on the local weather conditions. However, in some cases, the feed-water temperature was constant at its maximum value correspondent to the ambient temperature and insulation. Fig. 6 shows the variation of feed water temperatures on a selected day (13th December 2013) together with other parameters. The temperature reached its maximum value, about 56°C, between 1 and 2 p.m. The effect of decline of insolation is also noticeable on the feed-water temperature. The postponed influence is same as the time interval from the collector outlet to the membrane inlet. Therefore, it is illustrated that the operational conditions greatly affect the distribution of permeate flux in the system. Since the flow rate and pressure were kept constant, temperature of the feed solution is the main governing parameter that controls the distillate production.

#### 4.3. Sensitivity analysis of the model

The MATLAB program calculates the hourly rate of flux throughout a year. Sensitivity analysis has been performed by varying the vacuum pressure and feed flow rate as operating parameters. The effect of solar irradiance

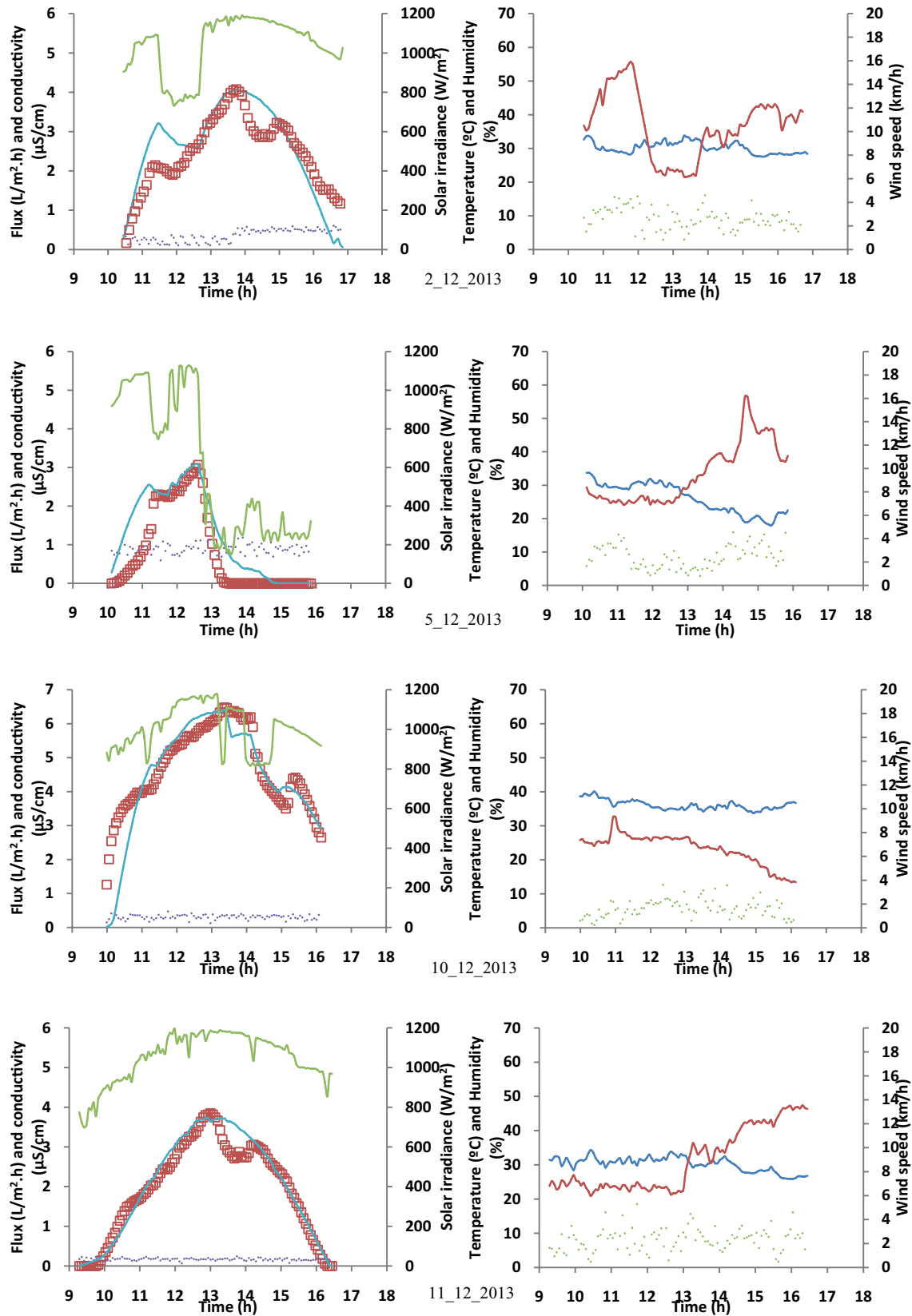


Fig. 5. The simulated rate of flux (—), experimental rate of flux (□), solar irradiance (---) and electrical conductivity (···) during a day together with ambient temperature (—), humidity (---) and wind speed (···). (Continued)

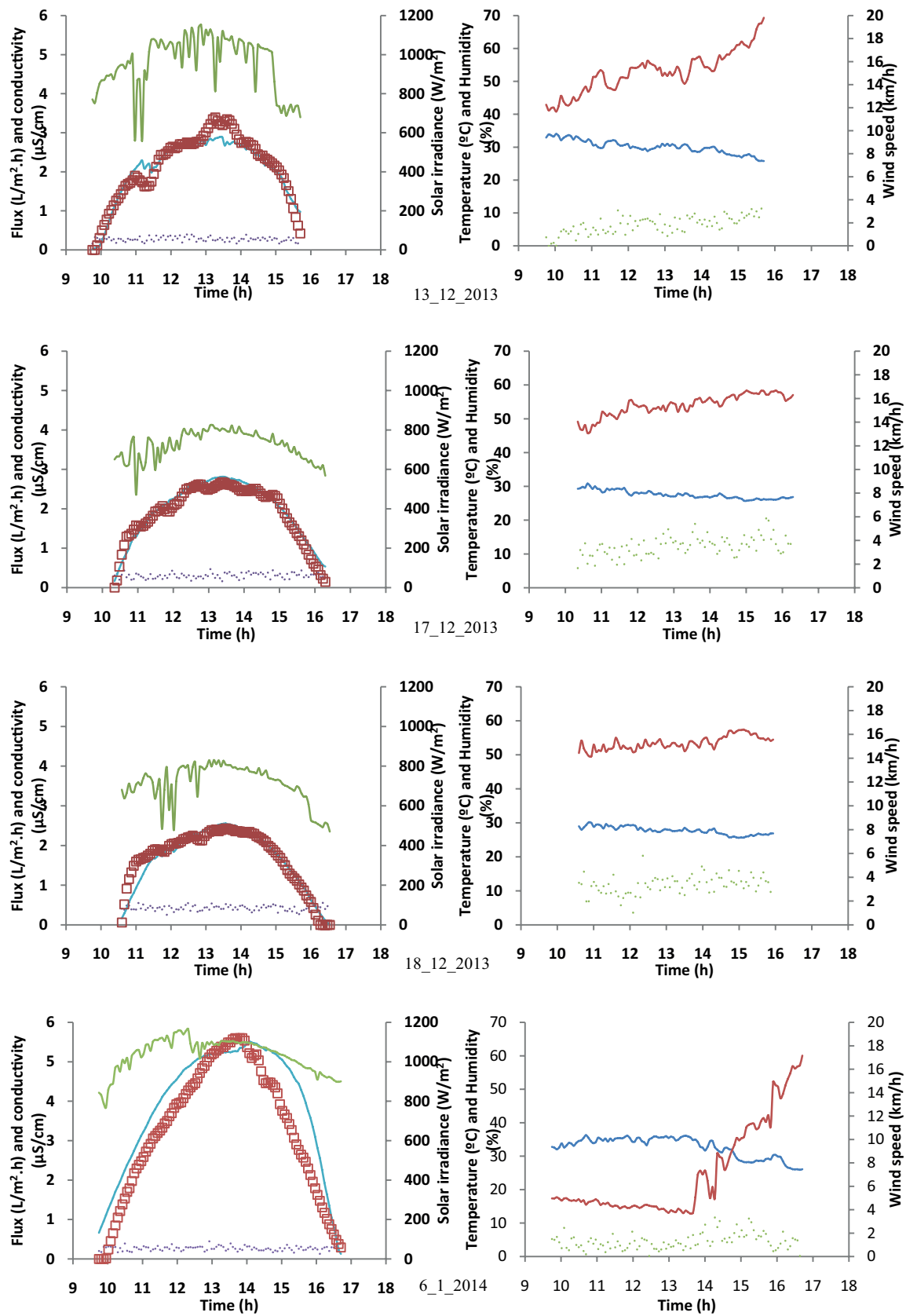


Fig. 5. (Continued) The simulated rate of flux (—), experimental rate of flux (□), solar irradiance (---) and electrical conductivity (···) during a day together with ambient temperature (—), humidity (---) and wind speed (···). (Continued)

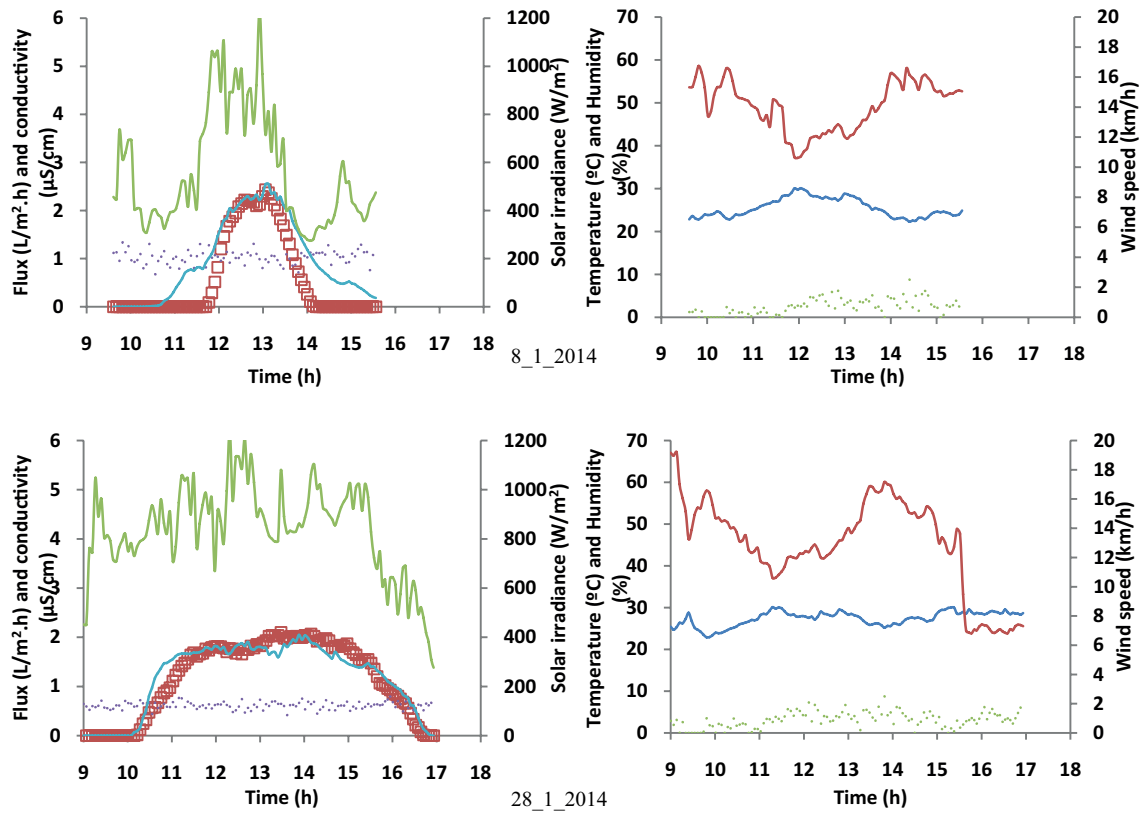


Fig. 5. (Continued) The simulated rate of flux (—), experimental rate of flux (□), solar irradiance (—) and electrical conductivity (···) during a day together with ambient temperature (—), humidity (—) and wind speed (···).

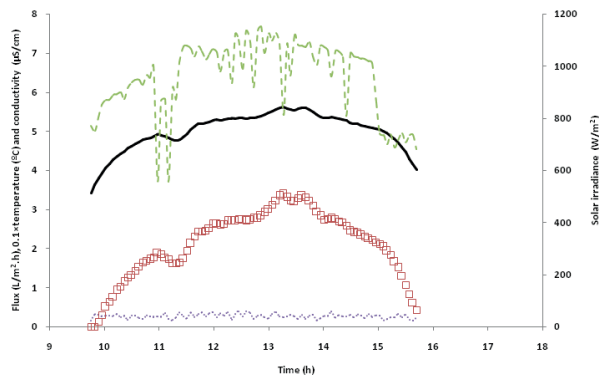


Fig. 6. The experimental rate of flux (□), feed-water temperature (—), solar irradiance (—) and electrical conductivity (···) on 13th of Dec 2013.

variation was also examined which is the most effective parameter that changes the feed-water temperature. Furthermore, membrane characteristics such as pore size and porosity were also tested. The assigned values for each parameter within the change of increase are shown in Table 1.

The results for sensitivity analysis are shown in Fig. 7. As predicted, the reduction of permeate side pressure and second loop flow rate and increase of solar irradiance, pore size and porosity can increase the rate of flux. Fig. 7(a) illustrates the influence of pressure variation on the permeate flux. A decrease of pressure by about 4 kPa from 10 kPa was useful to achieve 8%–16% more rate of flux. The rate of increase for permeate flux varies due to dynamic temperature values for feed water during a day and a year. On the other hand, when 10 kPa pressure was applied on the permeate side, the rates of permeate flux reduction were from 4% to 7%. This is also attributed to the variation of temperature during a day and a year.

Table 1  
Parameter range selected for sensitivity analysis

Parameter (Unit)	Pressure (kPa)	Flow rate (L min <sup>-1</sup> )	Solar irradiance (W m <sup>-2</sup> )	Pore size (µm)	Porosity (%)
Range	2–10	0.25–0.75	–	0.1–0.2	60–70
Rate of change	4	0.25	±200	0.05	5

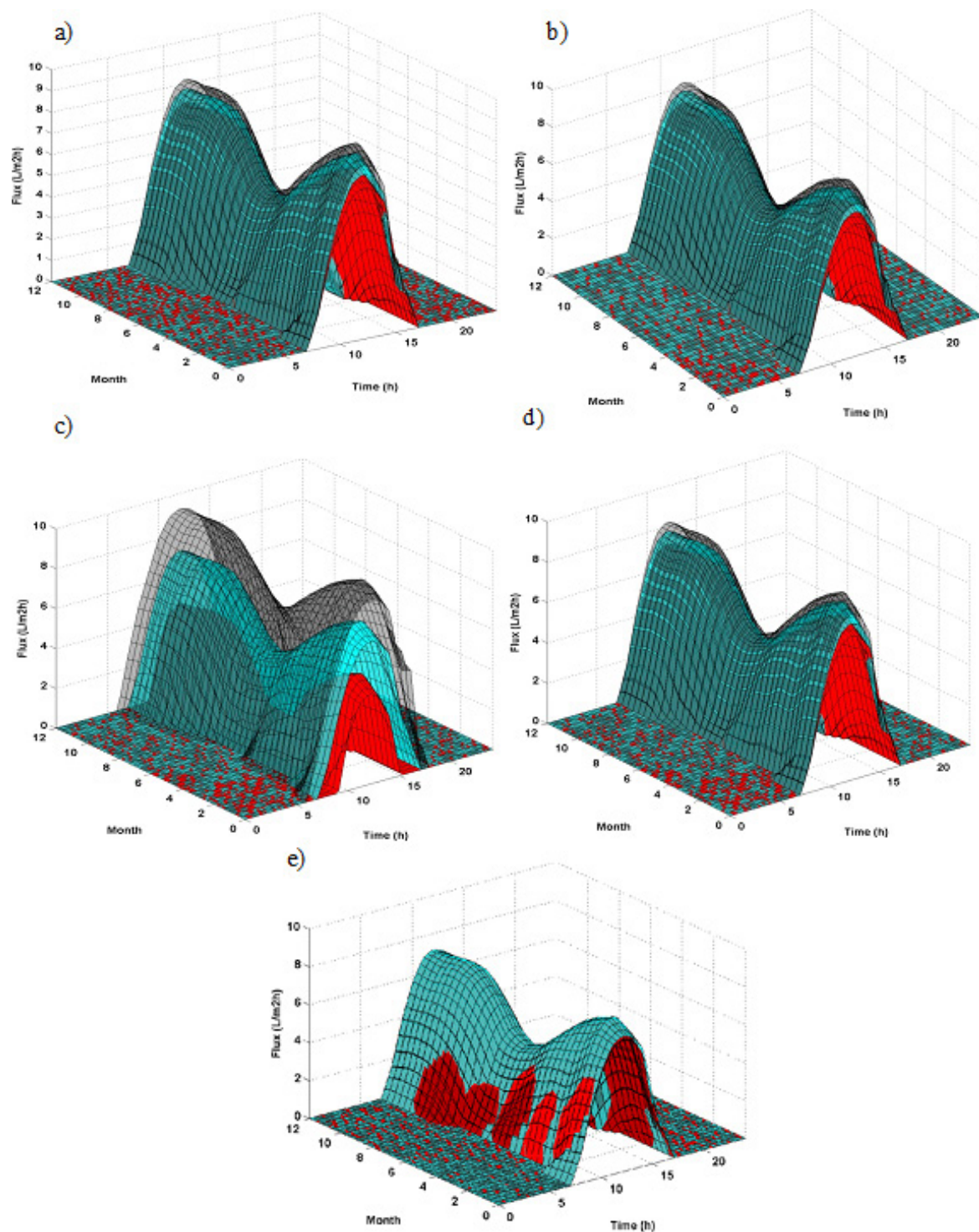


Fig. 7. The simulation model response to the variation of parameters indicated in Table 1: (a) the effect of vacuum pressure, (b) the effect of feed flow rate, (c) the effect of solar irradiance, (d) the effect of pore size and (e) the effect of porosity.

In this system, higher flow rates will decrease the contact time between the feed water and the solar collector. So, higher flow rates reduce the rate of heat absorption. Fig. 7(b) depicted that the lower flow rate will increase the rate of permeate flux, and vice versa. The permeate flux rate varies 10%–17% associated with the flow-rate changes of  $\pm 0.25 \text{ L min}^{-1}$ . The model

estimates a higher rate of flux at lower flow rates since the heat loss equation was not considered for the stream from the collector outlet to the membrane inlet. The main heat loss was applied for the reservoir which is placed after the membrane. To determine the optimum flow rate, accurate heat loss equation has to be incorporated.

The variation of solar irradiance by  $\pm 200 \text{ Wm}^{-2}$  significantly changes the feed water temperature. Fig. 7(c) shows that the increase of solar irradiance directly affects the growth rate of the permeate flux. There was no limit for temperature in this sensitivity analysis. The rate of the permeate flux varies between 29% and 100%. The highest rate of change is attributed to the points where the rate of the permeate flux is zero for the initial test. The SVM system operated with the initial solar irradiance  $200 \text{ Wm}^{-2}$  can obtain permeate flux earlier in the morning and end later in the afternoon due to the availability of enough solar irradiance.

Membrane pore size was also important for the achieved rate of the permeate flux. The permeate flux varies between 4% and 12% with the  $\pm 0.05 \mu\text{m}$  changes of the pore size. Larger pore size increases the rate of the permeate flux, however the pressure difference has to be maintained less than the LEP of the membrane. Fig. 7(d) shows the variation of flux for three different realistic pore sizes.

Membrane porosity plays the same role as the membrane pore size. Fig 7(e) illustrated the small effect of porosity by variation of  $\pm 5\%$  on the changes of rate of the permeate flux. It has marginal influence compared with the pore radius which is attributed to Eq. (28). The molar flux is directly influenced by the porosity of the membrane, and it is proportional to the membrane pore size. The fluctuation of the permeate flux rate varies between 0.2% and 1.5%.

#### 4.4. Influence of feed salinity

Two sets of experiments were performed for the effect of salinity concentration on the decline rate of the permeate flux using 5 and  $20 \text{ gL}^{-1}$  NaCl solutions. A 3-day test was carried out using  $5 \text{ gL}^{-1}$  saline solution from 13th to 15th January 2014. Experimental data along with the simulated model for  $5 \text{ gL}^{-1}$  saline solution are plotted in Fig. 8. The effect of feed-water salinity concentration on the flux

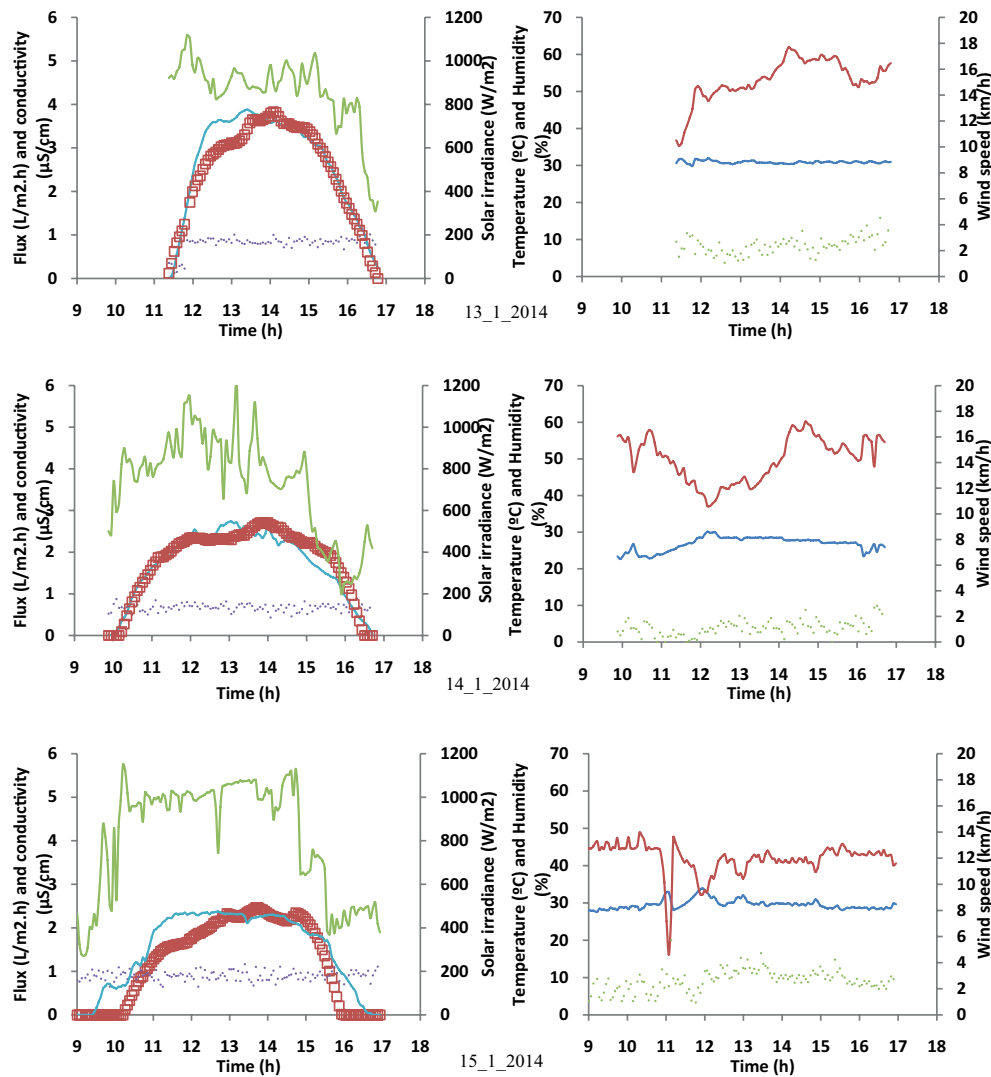


Fig. 8. The simulated rate of flux (—), experimental rate of flux (□), solar irradiance (---) and electrical conductivity (···) during a day together with ambient temperature (—), humidity (---) and wind speed (···) for a 3-day test with  $5 \text{ gL}^{-1}$  saline solution.

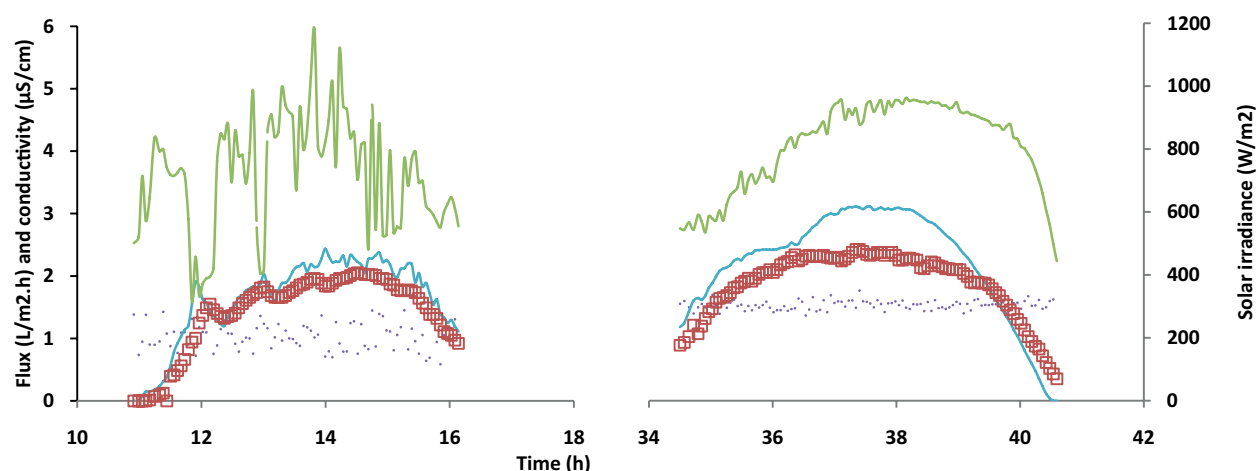


Fig. 9. The simulated rate of flux (—), experimental rate of flux (□), solar irradiance (---) and electrical conductivity (···) for a 3-day test with 20 g L<sup>-1</sup> saline solution.

performance was not observed. Although, the simulated model has some separation from the experimental data in a few points, the maximum values for the experimental permeate flux were similar to the simulated ones.

The SVMMD system was also used for desalination of 20 gL<sup>-1</sup> saline solution. A 2-day test was conducted during 16th and 17th January 2014. Fig. 9 presents the simulated permeate flux together with the experimental rate of flux. As expected, the salinity effect on the decline rate of the permeate flux was highlighted during the second day. Up to 15% discrepancy was derived between the simulated and the experimental flux rates for the first day. This difference was increased to 38% during the second day. Higher salinity concentration results in a remarkable decrease of the permeate flux rate which is correspondent to the open pore area reduction. Membrane cleaning procedure is required to take place for more than 20% reduction of permeate flux. Salt removal efficiency was always greater than 99.9%. Electrical conductivity values of the distillate water were excellent which is in the range of 0.6–1.6 µScm<sup>-1</sup>. This clearly shows that there is no pore wetting problem in the system.

## 5. Conclusion

A small scale VMD unit assisted by solar energy (SVMMD) was designed, built and examined. The performance of the SVMMD system utilized a number of temperature probes, pressure and flow sensors to evaluate the simulated model. The proposed model for the permeate flux was derived by the mathematical heat and/or mass transfer equations presented for each component used in the system. A simulated model of the system, has been developed, implemented in MATLAB and applied for the available average hourly data of Sydney. The model was then verified through the experimental results, and provides an acceptable description of the permeate flux. An experimental study was carried out for different feed solutions under real conditions. A meteorological station monitored solar irradiance, ambient temperature, humidity and wind speed each day. The SVMMD system shows that its performance is remarkably influenced

by the amount of energy transported to the feed water, since other operating parameters such as pressure and flow rate were kept constant. Maximum distillate flux varied from 2.1 to 6.5 Lm<sup>-2</sup>h<sup>-1</sup> during the two month tests. The variation of the permeate flux was the result of changes in feed-water temperature which was correspondent to solar irradiance, ambient temperature and wind speed. Subsequently, sensitivity analysis was performed for a set of significant parameters such as pressure, flow rate, solar irradiance, membrane pore size and membrane porosity. It has been shown that decrease of pressure and flow rate and increase of solar irradiance, membrane pore size and membrane porosity individually increases the flux rate.

Finally, the results for simulated and experimental permeate flux have been compared for desalination of 5 and 20 gL<sup>-1</sup> saline solutions. It was concluded that the low saline solution had an intangible effect on the rate of the permeate flux during a 3-day period. However, up to 38% difference between simulated and experimental data was observed for the 2-day test for 20 gL<sup>-1</sup> feed solution. The SVMMD system was able to remove salts from the solutions, and the electrical conductivity values of the distillate water were excellent in all cases which were in the range of 0.6–1.6 µScm<sup>-1</sup>.

## References

- [1] E. Guillén-Burrieza, G. Zaragoza, S. Miralles-Cuevas, J. Blanco, Experimental evaluation of two pilot-scale membrane distillation modules used for solar desalination, *J. Membr. Sci.*, 409–410 (2012) 264–275.
- [2] E. Mathioulakis, V. Belessiotis, E. Delyannis, Desalination by using alternative energy: review and state-of-the-art, *Desalination*, 203 (2007) 346–365.
- [3] J. Koschikowski, M. Wieghaus, M. Rommel, Solar thermal-driven desalination plants based on membrane distillation, *Desalination*, 156 (2003) 295–304.
- [4] M.R. Qtaishat, F. Banat, Desalination by solar powered membrane distillation systems, *Desalination*, 308 (2013) 186–197.
- [5] Y.-D. Kim, K. Thu, N. Ghaffour, Ng, K. Choon, Performance investigation of a solar-assisted direct contact membrane distillation system, *J. Membr. Sci.*, 427 (2013) 345–364.
- [6] M. Khayet, Membranes and theoretical modeling of membrane distillation: a review, *Adv. Colloid Interf. Sci.*, 164 (2011) 56–88.

- [7] M.S. El-Bourawi, Z. Ding, R. Ma, M. Khayet, A framework for better understanding membrane distillation separation process, *J. Membr. Sci.*, 285 (2006) 4–29.
- [8] J.P. Mericq, S. Laborie, C. Cabassud, Evaluation of systems coupling vacuum membrane distillation and solar energy for seawater desalination, *Chem. Eng. J.*, 166 (2010) 596–606.
- [9] H. Chen, C. Wu, Y. Jia, X. Wang, X. Lu, Comparison of three membrane distillation configurations and seawater desalination by vacuum membrane distillation, *Desal. Water Treat.*, 28 (2011) 321–327.
- [10] F. Banat, F.A. Al-Rub, K. Bani-Melhem, Desalination by vacuum membrane distillation: sensitivity analysis, *Separ. Purif. Technol.*, 33 (2003) 75–87.
- [11] S. Gabsi, A. Chehbouni, Solar Vacuum Membrane Distillation for Seawater Desalination, Paper Presented at the Renewable and Sustainable Energy Conference (IRSEC), 7–9 March 2013.
- [12] M. Khayet, T. Matsuura, Chapter 12 – Vacuum Membrane Distillation Membrane Distillation, Amsterdam: Elsevier, 2011, pp. 323–359.
- [13] G. Ramon, Y. Agnon, C. Dosoretz, Heat transfer in vacuum membrane distillation: effect of velocity slip, *J. Membr. Sci.*, 331 (2009) 117–125.
- [14] M. Sivakumar, M. Ramezani pour, G. O'Halloran, Mine water treatment using a vacuum membrane distillation system, *APCBEE Procedia*, 5 (2013) 157–162.
- [15] X. Wang, L. Zhang, H. Yang, H. Chen, Feasibility research of potable water production via solar-heated hollow fiber membrane distillation system, *Desalination*, 247 (2009) 403–411.
- [16] Z. Ding, L. Liu, M.S. El-Bourawi, R. Ma, Analysis of a solar-powered membrane distillation system, *Desalination*, 172 (2005) 27–40.
- [17] M. Elimelech, W.A. Phillip, The future of seawater desalination: energy, technology, and the environment, *Science*, 333 (2011) 712–717.
- [18] M. Khayet, Solar desalination by membrane distillation: dispersion in energy consumption analysis and water production costs (a review), *Desalination*, 308 (2013) 89–101.
- [19] F. Banat, N. Jwaied, M. Rommel, J. Koschikowski, M. Wieghaus, Desalination by a “compact SMADES” autonomous solar-powered membrane distillation unit, *Desalination*, 217 (2007) 29–37.
- [20] F. Banat, N. Jwaied, M. Rommel, J. Koschikowski, M. Wieghaus, Performance evaluation of the “large SMADES” autonomous desalination solar-driven membrane distillation plant in Aqaba, Jordan, *Desalination*, 217 (2007) 17–28.
- [21] M.C. de Andrés, J. Doria, M. Khayet, L. Peña, J.I. Mengual, Coupling of a membrane distillation module to a multieffect distiller for pure water production, *Desalination*, 115 (1998) 71–81.
- [22] J. Koschikowski, M. Wieghaus, M. Rommel, V.S. Ortin, B.P. Suarez, J.R.B. Rodríguez, Experimental investigations on solar driven stand-alone membrane distillation systems for remote areas, *Desalination*, 248 (2009) 125–131.
- [23] R.G. Raluy, R. Schwantes, V.J. Subiela, B. Peñate, G. Melián, J.R. Betancort, Operational experience of a solar membrane distillation demonstration plant in Pozo Izquierdo-Gran Canaria Island (Spain), *Desalination*, 290 (2012) 1–13.
- [24] C. Bier, U. Plantikow, Solar Powered Desalination by Membrane Distillation, Paper Presented at the IDA World Congress on Desalination and Water Science, Abu Dhabi, 1995.
- [25] J. Blanco Gálvez, L. García-Rodríguez, I. Martín-Mateos, Seawater desalination by an innovative solar-powered membrane distillation system: the MEDESOL project, *Desalination*, 246 (2009) 567–576.
- [26] R.B. Saffarini, E.K. Summers, H.A. Arafat, V.J.H. Lienhard, Economic evaluation of stand-alone solar powered membrane distillation systems, *Desalination*, 299 (2012) 55–62.
- [27] A. Cipollina, M.G. Di Sparti, A. Tamburini, G. Micale, Development of a membrane distillation module for solar energy seawater desalination, *Chem. Eng. Res. Design: Trans. Inst. Chem. Eng. Part A*, 90 (2012) 2101–2121.
- [28] P.A. Hogan, Sudjito, A.G. Fane, G.L. Morrison, Desalination by solar heated membrane distillation, *Desalination*, 81 (1991) 81–90.
- [29] F. Suárez, S.W. Tyler, A.E. Childress, A theoretical study of a direct contact membrane distillation system coupled to a salt-gradient solar pond for terminal lakes reclamation, *Water Res.*, 44 (2010) 4601–4615.
- [30] J. Walton, H. Lu, C. Turner, S. Solis, H. Herbert, Solar and Waste Heat Desalination by Membrane Distillation, University of Texas El Paso Desalination and Water Purification Research and Development Program 81, 2004.
- [31] S. Ben Abdallah, N. Frikha, S. Gabsi, Design of an autonomous solar desalination plant using vacuum membrane distillation, the MEDINA project, *Chem. Eng. Res. Design*, 91 (2013) 2782–2788.
- [32] R.B. Saffarini, E.K. Summers, H.A. Arafat, V.J.H. Lienhard, Technical evaluation of stand-alone solar powered membrane distillation systems, *Desalination*, 286 (2012) 332–341.
- [33] H. Wu, Y. Hou, Recent development of grid-connected PV systems in China, *Energy Procedia*, 12 (2011) 462–470.
- [34] T. Berrill, Australian solar radiation data handbook edition 4 [book review], *Austral. J. Environ. Educ.*, 23 (2007) 74–75.
- [35] M. Qtaishat, T. Matsuura, B. Kruczek, M. Khayet, Heat and mass transfer analysis in direct contact membrane distillation, *Desalination*, 219 (2008) 272–292.
- [36] G.C. Sarti, C. Gostoli, S. Bandini, Extraction of organic-components from aqueous streams by vacuum membrane distillation, *J. Membr. Sci.*, 80 (1993) 21–33.
- [37] B.E. Poling, J.M. Prausnitz, J.P. ÓConnell, *The Properties of Gases and Liquids*, 5th ed., McGraw Hill: New York, 2001.
- [38] K.W. Lawson, D.R. Lloyd, Membrane distillation, *J. Membr. Sci.*, 124 (1997) 1–25.
- [39] M. Khayet, T. Matsuura, Pervaporation and vacuum membrane distillation processes: modeling and experiments, *AIChE J.*, 50 (2004) 1697–1712.
- [40] J.I. Mengual, M. Khayet, M.P. Godino, Heat and mass transfer in vacuum membrane distillation, *Int. J. Heat Mass Transfer*, 47 (2004) 865–875.
- [41] C.M. Guijt, I.G. Rácz, T. Reith, A. de Haan, Determination of membrane properties for use in the modelling of a membrane distillation module, *Desalination*, 132 (2000) 255–261.